Electrochemical Impedance Simulation for Single Cell Analysis using a Microelectrode

Masataka Shiozawa and Shigeyasu Uno
Graduate School of Science and Engineering, Ritsumeikan University,
1-1-1 Noji-Higashi, Kusatsu, Shiga, 525-8577, Japan

Keywords: Electrochemical Impedance, Simulation, Single Cell Analysis, Microelectrode.

Abstract: Electrochemical impedance spectroscopy (EIS) is one of the ways to monitor living cells in terms of morphology and cell-substrate adhesion. In conventional cell analysis, averaged values from many cells on a large area electrode are acquired. Meanwhile, single cell characteristics are obtained by using a microelectrode which is smaller than single cell size. In this study, we investigated the impact of electrode size on single cell EIS analysis by using a computer simulation. The electrode smaller than the cell size would enable independent measurement of the cytoplasm electrical conductivity and the cell-substrate gap resistance. In addition, changes in morphology such as cell height and radius should be monitored at the same time in different frequency range. Thus, our simulation indicates that EIS measurement with microscale electrode may be used in monitoring various physiological changes in cells such as immune response.

1 INTRODUCTION

Nowadays, the living cell monitoring is used in disease diagnosis (Cheng et al., 2007) and drug discovery (Weigl et al., 2003). In drug discovery, the side effect on tissue culture is evaluated by monitoring cells. This method is used in regenerative medicine as well as in disease diagnosis and drug discovery. In regenerative medicine, one of the basic ways of treatment is to transplant the stem cell induced differentiation to the affected area. During inducing differentiation process, we need to monitor the morphological change of the stem cell to detect the progress of differentiation (Santelli et al., 2018). As mentions above, the living cell monitoring is needed in various areas.

The fluorescent labeling such as fluorescence microscope (Hopt & Neher, 2001) and flow cytometry (Nolan et al., 2018) has long been used as the way of monitoring living cells. These methods can selectively monitor any proteins and antigens due to staining. In addition, these methods can provide the quantitative information by estimating the fluorescent reflection signal from cells irradiated with excitation light (Hopt & Neher, 2001; Nolan et al., 2018). However, the fluorescent labeling may alter original characteristics of cells. In addition, the fluorescent labeling eventually induces the cell death. Thus, it is not appropriate to monitor the cells in long term, and therefore, the label-free monitoring methods have been explored.

There are some researches about the ways of monitoring living cells without labeling, such as Raman spectroscopy (Moura et al., 2016) and surface plasmon microscopy (Toma et al., 2014). The electrochemical impedance spectroscopy (EIS) is one of the applicable ways which require no labeling. Contrary to the fluorescent labeling, the EIS measurement is suitable to monitor in long term. In EIS measurement, the AC voltage of several mV is applied to the electrode. Then the electric current is measured, and impedance is calculated from the ratio of current to voltage to analyze the object. Previous studies have proven that the EIS measurement for cell analysis can supply various information such as the apoptosis, the movement of cancer cells through the tight junction of endothelial cells (Anchan et al., 2019), the wound healing (Gamal et al., 2019), the cell proliferation (Cui et al., 2017; Iwakura et al., 2019) and the cell migration (Cui et al., 2017; Iwakura et al., 2019) by sweeping frequency. The EIS measurement does not need any optical equipment. Therefore, the EIS measurement should be used in point of care (Hedayatipour et al., 2019; Ahmed et al., 2014) by downsizing the whole measurement system

Shiozawa, M. and Uno, S.
Electrochemical Impedance Simulation for Single Cell Analysis using a Microelectrode.
DOI: 10.5220/0010266401140120
In *Proceedings of the 14th International Joint Conference on Biomedical Engineering Systems and Technologies (BIOSTEC 2021) - Volume 1: BIODEVICES*, pages 114-120
ISBN: 978-989-758-490-9

with CMOS technology (Hedayatipour et al., 2019; Manickam et al., 2010).

In conventional cell analysis, cell characteristics are obtained from average values of many cells on a large electrode. However, recent study shows that cells may have the difference of gene. Hence, the individual cell difference such as the cell shape is caused (Moura et al., 2016). Such analysis ignores these individual cell differences (Zhou et al., 2010). On the other hand, single cell monitoring is a useful method because the individual cell differences can be observed (Zhou et al., 2010). In EIS measurement, various electrode structures have been used to measure; the interdigitated electrodes have long been used by many experimentalists as the electrochemical sensor (Ibrahim et al., 2013; Radke & Alocilja, 2005). Meanwhile, EIS using a microelectrode can provide more capability of label-free and single cell analysis than any other electrode structures. In fact, experimental demonstration of impedance mapping with microelectrode for tissues is reported (Vijay et al., 2016; Miccoli et al., 2019). Such microscale electrodes are proposed to be used in high sensitivity measurement and detailed analysis in single cell monitoring. Nevertheless, it is difficult to associate experimental EIS data with underlying changes in cell morphology. Such relation can be made clear by computer simulation.

In this work, we demonstrate computer simulation of EIS with microelectrode for single cell analysis. Our computer simulation reveals relationship between EIS data and cell morphology parameters. Our findings will benefit experimentalists in analysis of experimental data and optimization of sensor microelectrode design.

2 THEORY

The equivalent circuit is used to analyse in EIS measurement. Fig. 1(a) shows the equivalent circuit model of conventional parallel facing electrode (Tanaka et al., 2020), where the C_{dl} indicates the electrochemical double layer capacitance and the Z_{c} indicates the impedance between cell and substrate (Giaever & Keese, 1991). In addition, the R_{sol} indicates the solution resistance and the R_{gap} indicates the intercellular solution resistance. The electrical components of cells were described as cell membrane capacitance (C_{mem}) and cytoplasm resistance (R_{cyto}). Fig. 1(b) shows the schematic illustration of impedance magnitude-frequency characteristics from the equivalent circuit shown in Fig. 1(a). Note that, in bode plot, the slope of capacitance and resistance are

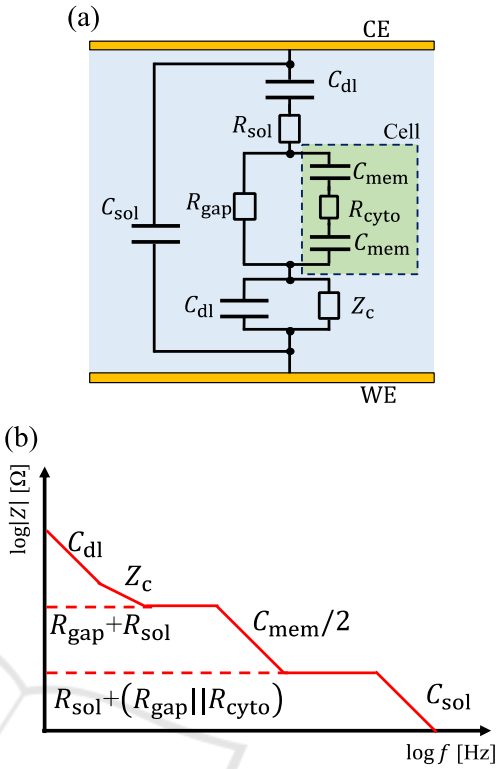

Figure 1: (a) The equivalent circuit model of parallel facing electrode for EIS measurement of cell. The WE and CE indicate working electrode and counter electrode, respectively. (b) Schematic illustration of impedance magnitude-frequency characteristics. The $(R_{\mathrm{gap}}||R_{\mathrm{cyto}})$ indicates the combined resistance of R_{gap} and R_{cyto} in parallel.

−1 and 0, respectively. On the other hand, the slope of Z_{c} is −1 or more, but less than 0 because the Z_{c} is expressed by the distributed model (Giaever & Keese, 1991). It should be noted that in this study, a microelectrode was used as working electrode (WE), and hence this equivalent circuit (Fig. 1(b)) is not exactly applicable to the analysis for this study. However, when we analyze the result of simulation for single cell on a microelectrode, we should obtain valuable information by comparing to this equivalent circuit.

3 IMPEDANCE CHARACTERISTICS FOR DISC ELECTRODE

The simulation model of single cell monitoring on a microelectrode is shown in Fig. 2(a). Constant bias was set to Zero and a sinusoidal voltage with

amplitude 5.0 mV was applied to WE while CE was set to ground. The cell was modeled as hemisphere (Ren & Chui, 2018) and the cell radius was set to 5µm. The distance between the WE and single cell was set to 100 nm (Ren & Chui, 2018). The mirror boundary condition was imposed on the side face of solution. Theoretical calculation with the following Eq. (1) is used to calculate the solution resistance in Fig. 2(a) (Denhoff, 2006).

$$R_S = \frac{1}{2\pi r_{we}\sigma}\arctan\left(\frac{2b}{r_{we}}\right), \quad (1)$$

where r_{we} is the WE radius, σ is the conductivity of solution and b is the distance between WE and CE. The simulated spreading resistance becomes analogous to the spreading resistance calculated by Eq. (1) under the condition that satisfies $r_{we} \ll b$ and $r_{we} \ll r_{ce}$, where r_{ce} is CE radius. Therefore, the distance between WE and CE was 100 times or more as long as WE radius. Likewise, CE radius was 100 times or more as long as WE radius. Actual simulation is done in axisymmetric 2D (cylindrical coordinate) as shown in Fig. 2(b) due to rotational symmetry. Table. 1 shows the parameters used in

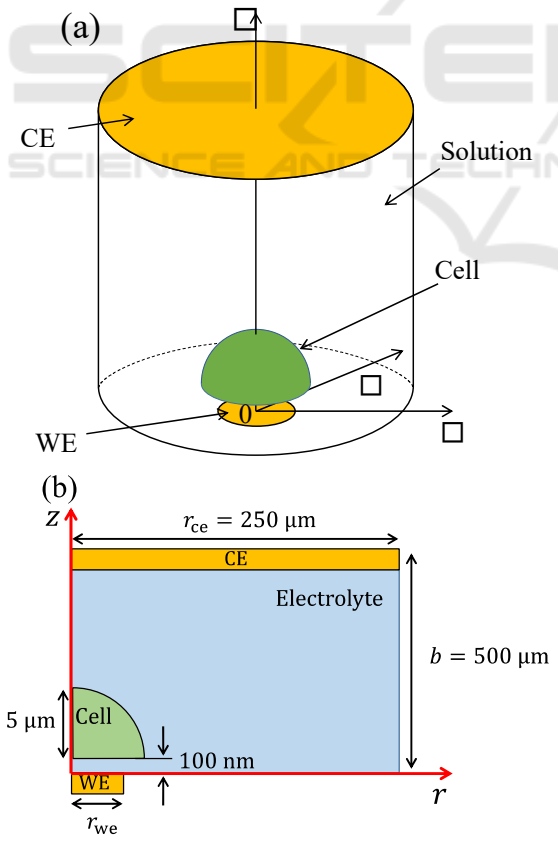

Figure 2: (a) Sensor structure, (b) simulation model in cylindrical coordinate.

swept from 10^2Hz to 10^9Hz. Note that the WE radius was changed from 2µm to 4.5µm stepped by 0.5µm. These WE radius were based on the literature of Miccoli et al (2019). We used COMSOL Multiphysics® 5.3a for numerical simulation. Note that the differentail forms of Maxwell's equations are solved in this software.

Table. 1: Parameter used in simulation (Ermolina et al., 2001).

Parameter	Value
Double layer capacitance per unit area [F/m^2]	0.89
Solution relative permittivity	78
Solution conductivity [S/m]	1.5
Cytoplasm relative permittivity	70
Cytoplasm conductivity [S/m]	1.0
Cell membrane thickness [nm]	5.0
Cell membrane relative permittivity	5.0
Cell membrane conductivity [S/m]	1.0×10^{-9}

3.1 Result

Fig. 3 shows the Bode plot of simulated impedance from Fig. 2(b). In Fig. 3, the electrical double layer capacitance (C_{dl}) is dominant around 10^3 Hz. From 10^4 Hz to 10^7 Hz, most of potential drops across solution between cell and sensor substrate, thus the cell-substrate impedance (Z_c) is dominant. Around 10^8 Hz, the impedance depends on the spreading resistance (R_S) (Denhoff, 2006), and the capacitance of solution is significant at 10^9 Hz. In Fig. 3, at 10^5 Hz, the slope of $|Z|$ becomes closer to 0 as r_{we} decreases. This behaviour is attributed to the fact that the equivalent circuit model of Z_c changes from distributed (Fig. 4(a)) (Giaever & Keese, 1991) to lumped-constant (Fig. 4(b)) model. This result indicates that the cell-substrate resistance could be detected directly, enabling to detect the change of conductivity between cell and sensor substrate. In higher frequency range around 10^8 Hz, the slope of $|Z|$ is almost 0. The impedance of cell membrane capacitance can be ignored here, and the impedance only depends on spreading resistance R_s (Denhoff, 2006). Fig. 5 represents impedance characteristics for disk microelectrode around 50 MHz. Note that in Fig. 5, the theoretical curve is calculated using the R_s formula with cytoplasm and solution conductivity. In Fig. 5, as r_{we} decreases, the simulated impedance becomes closer to the theoretical curve calculated by cytoplasm conductivity. This is attributed to the

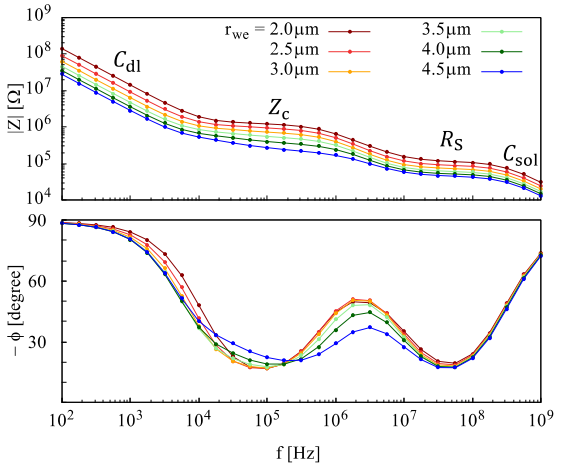

Figure 3: Bode plot of simulated impedance from Fig. 2. Legends indicate working electrode radius.

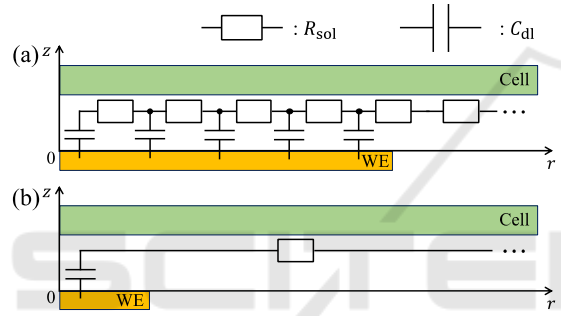

Figure 4: Schematic illustration of the equivalent circuit model of the impedance Z_C between cell and sensor substrate. (a) WE radius is close to cell radius and (b) WE radius is much smaller than cell radius.

potential drop localization around WE due to the decrease in r_{we}. Consequently, most of R_s becomes the spreading resistance within the cell. Hence, for smaller r_{we}, the impedance around 10^8Hz reflects the cytoplasm conductivity. This indicates that a microelectrode could reveal the conductivity inside the cell.

4 CELL ADHESION

The cell adhesion is an important behaviour in the healing process and immune response of tissues (Wegener et al., 2000). Hence, we simulated the cell adhesion process by using a microelectrode. Fig. 6(a) represents the simulation model of cell adhesion. In Fig. 6(a), the r_c was swept parametrically while the cell volume is fixed. Obviously, in Fig. 6(a), the radius and the height of cell change simultaneously. Therefore, another simulation as shown in Fig. 6(b)

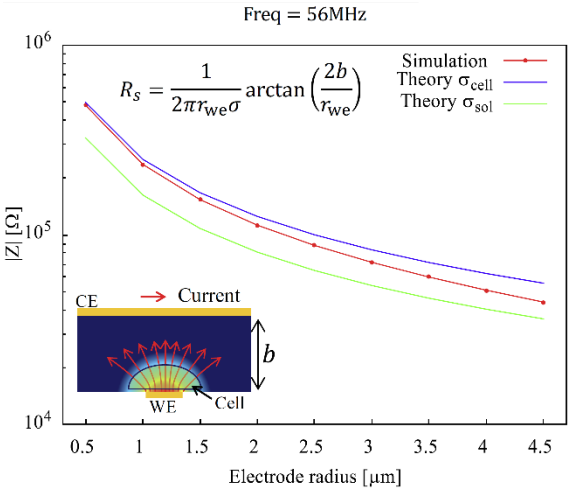

Figure 5: Electrode radius-impedance characteristics at 56 MHz and schematic illustration of electric potential and current flow. Electric potential drops from red to blue.

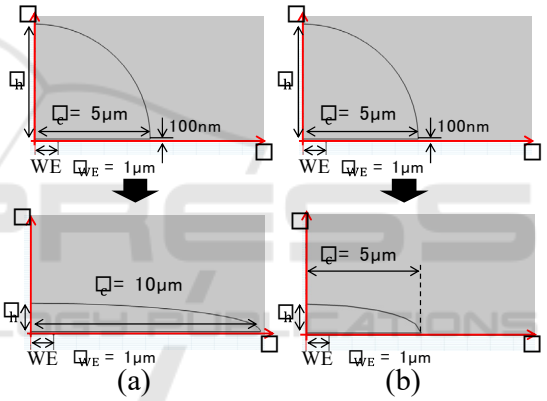

Figure 6: (a) Constant cell volume, (b) constant cell radius.

was done in order to identify which change has an impact on impedance by sweeping only r_h. In Fig. 6(b), the r_c is fixed to 5μm and the r_h is the same as used in Fig. 6(a). Note that the WE radius was set to 1μm because from the result in Fig. 5, we predicted that the smaller electrode should provide more sensitive detection of the cell height change in adherent process. The other parameters are the same as Table. 1.

4.1 Result

Figs. 7(a) and 7(b) represent the Bode plot of simulated impedance from Fig. 6(a) and Fig. 6(b), respectively. Fig. 7(c) represents the impedance sensitivity calculated based on Fig. 6(a). The sensitivity is written as

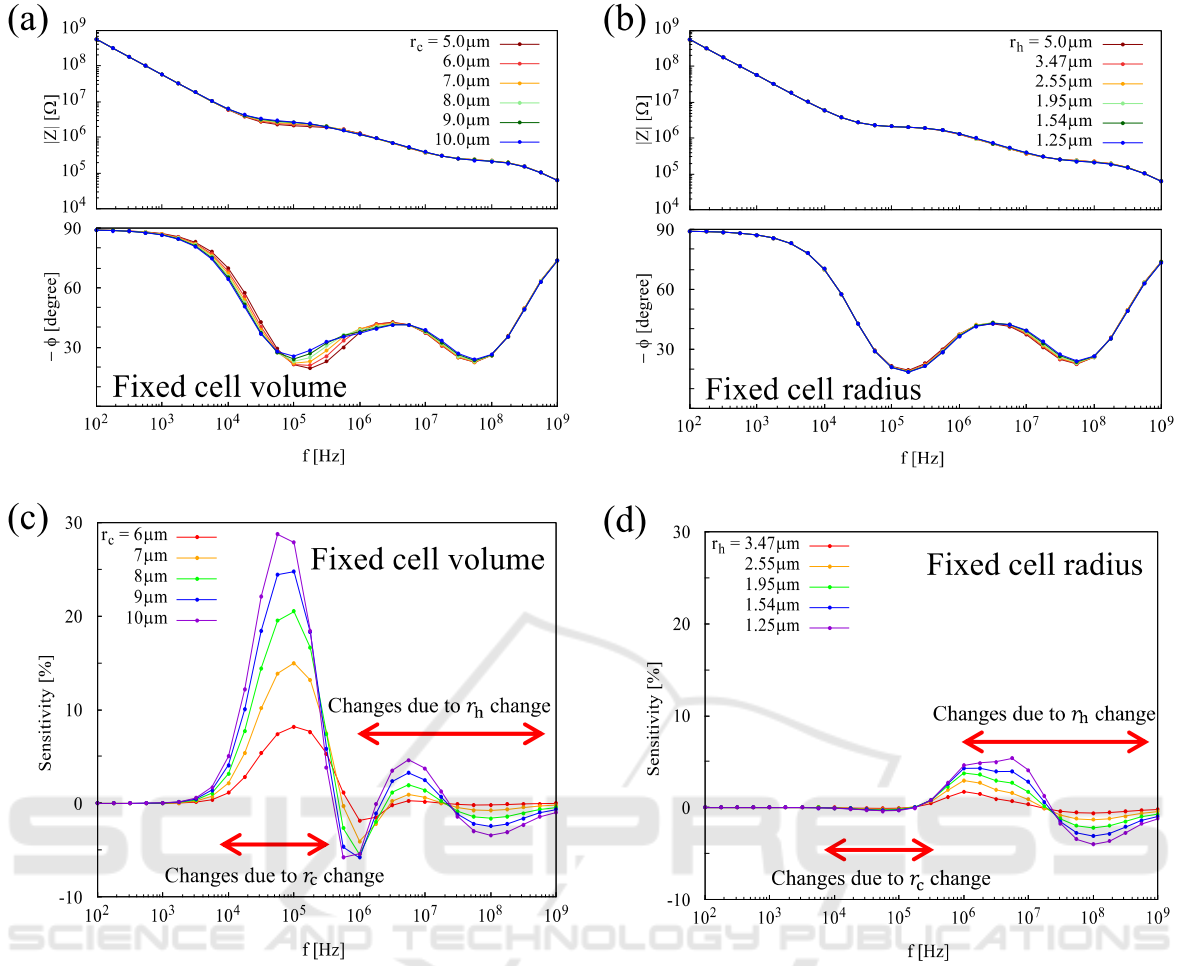

Figure 7: (a) Bode plot of simulated impedance from Fig.6(a). (b) Bode plot of simulated impedance from Fig.6(b). (c) Sensitivity calculated based on cell radius 5μm from (a), and (d) sensitivity calculated based on cell height 5μm from (b). Legends of (a), (c) indicate the cell radius and legends of (b), (d) indicate the cell height.

$$\text{Sensitivity [\%]} = \frac{|Z_r| - |Z_{5\mu m}|}{|Z_{5\mu m}|} \times 100\,, \qquad (2)$$

where $|Z_{5\mu m}|$ is the impedance magnitude when the cell radius is 5μm and $|Z_r|$ is the impedance magnitude of each cell radius except for 5μm. Likewise, Fig. 7(d) represents the impedance sensitivity from Fig. 7(b). Note that the peak sensitivity was achieved around 10^5 Hz in Fig. 7(c). This is attributed to the increase in cell-substrate resistance due to the increase in cell radius, which should not appear in Fig. 7(d) as expected. In other words, it is possible to measure independently the cell radius and cell height from the impedance for each frequency range.

5 DISCUSSION

In this study, we showed the benefit of using microelectrodes smaller than single cell size by computer simulation. The first point to be discussed is the impact of electrode size. In Fig. 3, around 10^5 Hz, smaller electrode size leads to more distinct detection of cell-substrate resistance. There is a report showing impedance change of aspirin-treated cell around 10^5 Hz (Yin et al., 2007), where the cells treated with 1mM aspirin showed the difference from the cells without treatment in the methyl tetrazolium (MTT) assay. On the other hand, in EIS measurement using electrode larger than single cell, there was no difference between the treated cell and the control cell. The microelectrode could provide the difference of impedance magnitude between the cells treated with

1mM aspirin and the cells without treatment around 10^5 Hz. In Fig. 5, around 10^8 Hz, as the electrode size decreases, the simulated impedance becomes closer to the theoretical curve calculated using the R_s formula with cytoplasm conductivity. This result indicates that the theoretical value can provide the cytoplasm electrical conductivity. Previous study shows the measurement of cytoplasm impedance changes under the different concentrations of drug introduced into cells (Stolwijk et al., 2011). The concentration of drug could be surmised from cytoplasm electrical conductivity by using a microelectrode. The second concerns the change in morphology such as cell height and radius. Figs. 7(c) and 7(d) show that the electrode smaller than single cell size can provide the significant sensitivity to detect the morphological change of single cell. A recent study showed that the impedance change was caused by the morphological change derived from cellular differentiation (Hildebrandt et al., 2010). However, the difference of impedance magnitude between control and necrotic spheroids was 6% at most (Hildebrandt et al., 2010). It is quite possible that using microscale electrode instead of the electrode having a diameter of 1mm affords the significant difference of impedance magnitude in the same experiment.

6 CONCLUSIONS

The simulation was performed to study the characteristics of a microelectrode smaller than single cell. First, a microelectrode shows the feasibility to measure the resistance between cell and substrate at low frequency. Second, microelectrode smaller than a cell shows better performance in detection the conductivity inside the cell at high frequency. The simulation of the cell adhesion process showed that a microelectrode exhibits sufficient sensitivity to measure the radius and the height of cell independently in different frequency range.

ACKNOWLEDGEMENTS

This work was supported by JSPS KAKENHI 19K04539.

REFERENCES

Cheng, X., Liu, Y., Irimia, D., Demirci, U., Yang, L., Zamir, L., … Bashir, R. (2007). Cell detection and counting through cell lysate impedance spectroscopy in microfluidic devices. *Lab Chip*, *7* (6), 746–755.

Weigl, B. H., Bardell, R. L., & Cabrera, C. R. (2003). Lab-on-a-chip for drug development. *Advanced Drug Delivery Reviews*, *55* (3), 349–377.

Santelli, J., Lechevallier, S., Baaziz, H., Vincent, M., Martinez, C., Mauricot, R., … Cussac, D. (2018). Multimodal gadolinium oxysulfide nanoparticles: a versatile contrast agent for mesenchymal stem cell labeling. *Nanoscale*, *10* (35), 16775–16786.

Hopt, A., & Neher, E. (2001). Highly Nonlinear Photodamage in Two-Photon Fluorescence Microscopy. *Biophysical Journal*, *80* (4), 2029–2036.

Nolan, J., Nedosekin, D. A., Galanzha, E. I., & Zharov, V. P. (2018). Detection of Apoptotic Circulating Tumor Cells Using in vivo Fluorescence Flow Cytometry. *Cytometry Part A*, *95* (6), 664–671.

Moura, C. C., Tare, R. S., Oreffo, R. O. C., & Mahajan, S. (2016). Raman spectroscopy and coherent anti-Stokes Raman scattering imaging: prospective tools for monitoring skeletal cells and skeletal regeneration. *Journal of The Royal Society Interface*, *13* (118), 20160182.

Toma, K., Kano, H., & Offenhäusser, A. (2014). Label-Free Measurement of Cell–Electrode Cleft Gap Distance with High Spatial Resolution Surface Plasmon Microscopy. *ACS Nano*, *8* (12), 12612–12619.

Anchan, A., Kalogirou-Baldwin, P., Johnson, R., Kho, D. T., Joseph, W., Hucklesby, J., … Graham, E. S. (2019). Real-Time Measurement of Melanoma Cell-Mediated Human Brain Endothelial Barrier Disruption Using Electric Cell-Substrate Impeda-nce Sensing Technology. *Biosensors*, *9* (2), 56.

Gamal, W., Borooah, S., Smith, S., Underwood, I., Srsen, V., Chandran, S., … Dhillon, B. (2015). Real-time quantitative monitoring of hiPSC-based model of macular degeneration on Electric Cell-substrate Impedance Sensing microelectro-des. *Biosensors and Bioelectronics*, *71*, 445–455.

Cui, Y., An, Y., Jin, T., Zhang, F., & He, P. (2017). Real-time monitoring of skin wound healing on nano-grooves topography using electric cell-substrate impedance sensing (ECIS). *Sensors and Actuators B: Chemical*, *250*, 461–468.

Iwakura, T., Marschner, J. A., Zhao, Z. B., Świderska, M. K., & Anders, H.-J. (2019). Electric cell-substrate impedance sensing in kidney research. *Nephrology Dialysis Transplantation*.

Hedayatipour, A., Aslanzadeh, S., & Mcfarlane, N. (2019). CMOS based whole cell impedance sensing: Challenges and future outlook. *Biosensors and Bioelectronics*, *143*, 111600.

Ahmed, A., Rushworth, J. V., Hirst, N. A., & Millner, P. A. (2014). Biosensors for Whole-Cell Bacterial Detection. *Clinical Microbiology Reviews*, *27* (3), 631–646.

Manickam, A., Chevalier, A., Mcdermott, M., Ellington, A. D., & Hassibi, A. (2010). A CMOS Electrochemical Impedance Spectroscopy (EIS) Biosensor Array. *IEEE Transactions on Biomedical Circuits and Systems*, *4* (6), 379–390.

Zhou, Y., Basu, S., Laue, E., & Seshia, A. A. (2016). Single cell studies of mouse embryonic stem cell (mESC) differentiation by electrical impedance measurements in a microfluidic device. *Biosensors and Bioelectronics*, *81*, 249–258.

Ibrahim, M., Claudel, J., Kourtiche, D., & Nadi, M. (2013). Geometric parameters optimization of planar interdigitated electrodes for bioimpedance spectroscopy. *Journal of Electrical Bioimpedance*, *4* (1), 13–22.

Radke, S. M., & Alocilja, E. C. (2005). A high density microelectrode array biosensor for detection of E. coli O157:H7. *Biosensors and Bioelectronics*, *20* (8), 1662–1667.

Vijay, V., Raziyeh, B., Amir, S., Jelena, D., Alicia, B. J., Axel, B., … Andreas, H. (2016). High-density CMOS microelectrode array system for impedance spectroscopy and imaging of biological cells. *2016 Ieee Sensors*.

Miccoli, B., Lopez, C. M., Goikoetxea, E., Putzeys, J., Sekeri, M., Krylychkina, O., … Braeken, D. (2019). High-Density Electrical Recording and Impedance Imaging With a Multi-Modal CMOS Multi-Electrode Array Chip. *Frontiers in Neuroscience*, *13*.

Tanaka, S., Kimura, K., Miyamoto, K., Yanase, Y., & Uno, S. (2020). Simulation and Experiment for Electrode Coverage Evaluation by Electrochemical Impedance Spectroscopy Using Parallel Facing Electrodes. *Analytical Sciences*, *36* (7), 853–858.

Giaever, I., & Keese, C. R. (1991). Micromotion of mammalian cells measured electrically. *Proceedings of the National Academy of Sciences*, *88* (17), 7896–7900.

Ren, D., & Chui, C. O. (2018). Feasibility of Tracking Multiple Single-Cell Properties with Impedance Spectroscopy. *ACS Sensors*, *3* (5), 1005–1015.

Denhoff, M. W. (2006). An accurate calculation of spreading resistance. *Journal of Physics D: Applied Physics*, *39* (9), 1761–1765.

Ermolina, I., Polevaya, Y., Feldman, Y., Ginzburg, B.-Z., & Schlesinger, M. (2001). Study of normal and malignant white blood cells by time domain dielectric spectroscopy. *IEEE Transactions on Dielectrics and Electrical Insulation*, *8* (2), 253–261.

Wegener, J., Keese, C. R., & Giaever, I. (2000). Electric Cell–Substrate Impedance Sensing (ECIS) as a Noninvasive Means to Monitor the Kinetics of Cell Spreading to Artificial Surfaces. *Experimental Cell Research*, *259* (1), 158–166.

Yin, H., Wang, F. L., Wang, A. L., Cheng, J., & Zhou, Y. (2007). Bioelectrical Impedance Assay to Monitor Changes in Aspirin-Treated Human Colon Cancer HT-29 Cell Shape during Apoptosis. *Analytical Letters*, *40* (1), 85–94.

Stolwijk, J. A., Hartmann, C., Balani, P., Albermann, S., Keese, C. R., Giaever, I., & Wegener, J. (2011). Impedance analysis of adherent cells after in situ electroporation: Non-invasive monitoring during intracellular manipulations. *Biosensors and Bioelectronics*, *26* (12), 4720–4727.

Hildebrandt, C., Büth, H., Cho, S., Impidjati, & Thielecke, H. (2010). Detection of the osteogenic differentiation of mesenchymal stem cells in 2D and 3D cultures by electrochemical impedance spectroscopy. *Journal of Biotechnology*, *148* (1), 83–90.